# Mechanism of Zinc Coordination by Point-Mutated Structures of the Distal CCHC Binding Motif of the HIV-1 NCp7 Protein†

Elisa Bombarda,‡,§ Bernard P. Roques,|| Yves Mély,*,‡ and Ernst Grell*,§

*UMR 7034 du CNRS, Laboratoire de Pharmacologie et Physico-Chimie des Interactions Cellulaires et Moléculaires, Faculté de Pharmacie, Université Louis Pasteur, 74, Route du Rhin, F-67401 Illkirch Cedex, France, Laboratoire de Pharmacochimie Moléculaire et Structurale, INSERM U266, CNRS FRE 2463, Faculté de Pharmacie, 4, Avenue de l'Observatoire, 75270 Paris Cedex 06, France, and Max-Planck-Institut für Biophysik, Max-von-Laue Strasse 3, 60438 Frankfurt, Germany*

*Received December 17, 2004; Revised Manuscript Received March 15, 2005*

ABSTRACT: The kinetics of $Zn^{2+}$ binding by two point-mutated forms of the HIV-1 NCp7 C-terminal zinc finger, each containing tridentate binding motif HCC [Ser49(35−50)NCp7] or CCC [Ala44(35−50)-NCp7], has been studied by stopped-flow spectrofluorimetry. Both the formation and dissociation rate constants of the complexes between $Zn^{2+}$ and the two model peptides depend on pH. The results are interpreted on the basis of a multistep reaction model involving three $Zn^{2+}$ binding paths due to three deprotonated states of the coordinating motif, acting as monodentate, bidentate, and tridentate ligands. For Ser49(35−50)NCp7 around neutral pH, binding preferentially occurs via the deprotonated Cys36 in the bidentate state also involving His44. The binding rate constants for the monodentate and bidentate states are $1 \times 10^6$ and $3.9 \times 10^7$ $M^{-1}$ $s^{-1}$, respectively. For Ala44(35−50)NCp7, intermolecular $Zn^{2+}$ binding predominantly occurs via the deprotonated Cys36 in the monodentate state with a rate constant of $3.6 \times 10^7$ $M^{-1}$ $s^{-1}$. In both mutants, the final state of the $Zn^{2+}$ complex is reached by subsequent stepwise ligand deprotonation and intramolecular substitution of coordinated water molecules. The rate constants for the intermolecular binding paths of the bidentate and tridentate states of Ala44(35−50)-NCp7 and of the tridentate state of Ser49(35−50)NCp7 are much smaller than expected according to electrostatic considerations. This is attributed to conformational constraints required to achieve proper metal coordination during folding. The dissociation of $Zn^{2+}$ from both peptides is again characterized by a multistep process and takes place fastest via the protonated $Zn^{2+}$-bound bidentate and monodentate states, with rate constants of ∼0.3 and $\sim 10^3$ $s^{-1}$, respectively, for Ser49(35−50)NCp7 and $\sim 4 \times 10^{-3}$ and ∼500 $s^{-1}$, respectively, for Ala44(35−50)NCp7.

Among the naturally selected metal cations, $Zn^{2+}$ displays a large variety of structural and catalytic roles (*1*). One of the most striking examples of its structural role is represented by the zinc finger proteins, where folding is completely linked to metal coordination. Here, $Zn^{2+}$ binding provides a favorable driving force directing the folding of the polypeptide chain from its unfolded to its functional, highly constrained structure (*2*−*6*). The folded conformation of the complex is required to promote selective nucleic acid binding, representing one principal function of zinc finger proteins. The tetrahedrally coordinated metal binding domain of each zinc finger protein consists generally of Cys-His arrays, such as CCHH, CCCC, and CCHC (*7*, *8*). Among the known CCHC motifs, the C-$X_2$-C-$X_4$-H-$X_4$-C sequence (X being a variable amino acid residue) is found to be the shortest. It is also termed the retroviral type zinc finger because it is found in all retroviral nucleocapsid proteins (NCps), with the only exception being spumaretrovirus. Additionally, this motif is present in the coat protein of the cauliflower mosaic virus, a protein of the *Drosophila* transposable element *copia*, and some human cellular nucleic acid binding proteins. A common feature of all proteins containing the retroviral CCHC motif is their involvement in sequence-specific single-stranded nucleic acid interactions (*9*, *10*).

The nucleocapsid protein of HIV-1, NCp7, is crucially involved in several key steps of the viral life cycle (RNA packaging, reverse transcription, and integration) through interactions with single-stranded nucleic acids and viral proteins (*11*−*16*). The binding of $Zn^{2+}$ to its two retroviral CCHC motifs and the proper folding of these motifs are found to be critical for the major functions of NCp7. Indeed, amino acid mutations that prevent or affect $Zn^{2+}$ binding induce the formation of noninfectious particles (*17*−*22*). The critical role of NCp7 zinc fingers in multiple phases of the HIV-1 replication cycle together with the occurrence of

† This work was supported by funds from Max-Planck-Institut für Biophysik, Agence Nationale de Recherches sur le SIDA, Sidaction, Centre National de la Recherche Scientifique, European Community (TRIoH integrated project), and Université Louis Pasteur. E.B. is grateful to the DAAD and Boehringer-Ingelheim Foundation for providing fellowships. Y.M. has been awarded an Alexander von Humboldt fellowship.

* To whom correspondence should be addressed. E.G.: e-mail, ernst.grell@mpibp-frankfurt.mpg.de; telephone, +49 (0)69 6303 24 00; fax, +49 (0)69 6303 24 02. Y.M.: e-mail, mely@pharma.u-strasbg.fr; telephone, +33 (0)3 90 24 42 62; fax, +33 (0)3 90 24 43 12.

‡ Université Louis Pasteur.

§ Max-Planck-Institut für Biophysik.

|| CNRS FRE 2463.

10.1021/bi047349+ CCC: $30.25 
Published on Web 04/23/2005

highly conserved residues in their sequence makes these domains attractive targets for antiviral drugs (*23*−*26*). In this context, the knowledge of the molecular coordination mechanism involved in zinc finger folding will not only be of fundamental scientific relevance but also help in the development of new strategies for impairing $Zn^{2+}$ binding. However, except for some initial studies related to the CCHC zinc finger motifs (*27*, *28*), no detailed report about the kinetics of metal binding by a zinc finger peptide has been published so far.

In a previous study, we have characterized the equilibrium $Zn^{2+}$ binding properties of the C-terminal CCHC motif of NCp7 as a simple but relevant model of the retroviral CCHC motifs (*29*−*31*). Metal ion coordination is markedly pH-dependent. Moreover, it has been suggested that the significant differences in the degree of deprotonation of the four coordinating residues lead to a nearly sequential, stepwise binding process (*30*).

To understand the dynamics of binding and thus also the mechanistic aspects, we report here a detailed kinetic $Zn^{2+}$ binding study at different pH values for two point-mutated forms of the C-terminal zinc finger motif of NCp7. The time course of the reaction was followed by the stopped-flow technique under anaerobic conditions using the intrinsic fluorescence of the naturally occurring Trp37 residue of the peptide. Mutated proteins are commonly used to investigate the folding mechanism and determine the involvement of intermediates or transition states (*32*, *33*). Therefore, in the study presented here, we have investigated the relationship between metal binding and peptide folding for two characteristic point-mutated peptides, Ser49(35−50)NCp7 and Ala44(35−50)NCp7 (cf. Chart 1; mutated residues are underlined) that have been shown previously to bind $Zn^{2+}$ with high affinity (*31*). These peptides act as tridentate ligands, where the originally occurring Cys49 in the former and His44 in the latter peptide have been substituted with noncoordinating serine and alanine, respectively.

Chart 1

Ala44(35-50)NCp7

H-GCWKCGKEG**A**QMKDCT-OH

Ser49(35-50)NCp7

H-GCWKCGKEGHQMKD**S**T-OH

Our data clearly indicate that $Zn^{2+}$ binding and dissociation have to be considered multistep processes, where intermediate states are involved in the reaction path under physiological conditions. Moreover, the mechanistic analysis of the mutated peptides investigated here provides relevant clues for the interpretation of the more complex binding behavior of the native peptide. Indeed, it is thought that the intermediates and the final state formed upon complex formation between $Zn^{2+}$ and the tridentate mutant peptides will also be involved in $Zn^{2+}$ coordination by the natural, tetradentate (35−50)NCp7 peptide.

## MATERIALS AND METHODS

*Materials and Preparation of Solutions*. The point-mutated analogues of the (35−50)NCp7 peptide, Ser49(35−50)NCp7 and Ala44(35−50)NCp7, were synthesized in their apo form as previously described (*34*). The buffers were chosen to cover the following pH ranges: *N*,*N*′-diethyl-*N*,*N*′-bis-(sulfopropyl)ethylenediamine (DESPEN, GFS Chemicals) for pH 4.7−5.6, 2-(*N*-morpholino)ethanesulfonic acid (MES, Microselect for luminescence, Fluka) for pH 5.6−6.8, and 4-(2-hydroxyethyl)piperazine-1-ethanesulfonic acid (HEPES, Microselect, Fluka) for pH 6.8−8.5. To minimize interactions between electrolyte anions and free or bound zinc ions, perchlorate salts were used. The ionic strength was always fixed by addition of $NaClO_4$ (purissimum p.a., Fluka). The pH of the solutions was adjusted with concentrated NaOH and $HClO_4$ (Suprapur, Merck). The $Zn^{2+}$-containing titrant solutions were prepared with $Zn(ClO_4)_2$ and degassed prior to use. All the solutions were prepared in LDPE (low-density polyethylene) flasks using Milli-Q (Millipore) filtered water (>17 MΩ/cm). The experimental conditions were such that hydrolysis of zinc ions was prevented. The peptides were dissolved in degassed buffer and kept in quartz cells (Hellma) under an argon atmosphere. The SH content of the free peptides during the experiments was decreased by less than 15% as checked by titration with 5,5′-dithiobis(2-nitrobenzoic acid) (DTNB, Fluka) (*35*, *36*).

*Absorption and Fluorescence Spectroscopy*. Peptide concentrations were determined from the absorption spectra recorded on a Cary 100 (Varian) or HP8450A (Hewlett-Packard) double-beam spectrophotometer, using a molar extinction coefficient of 5700 $M^{-1}$ $cm^{-1}$ at 280 nm. Fluorescence spectra were recorded with a Fluorolog 212 (Spex) spectrofluorimeter, equipped with a thermostated cuvette holder. Excitation was set to 280 nm. Excitation and emission bandwidths were 4 nm. The temperature was fixed at 20 ± 0.5 °C. An inert argon atmosphere was maintained inside the sample cell all over the measurements.

*Stopped-Flow Binding Kinetics*. Kinetic measurements were performed on a DX 17MV stopped-flow instrument (Applied Photophysics) using absorption and fluorescence detection (R1104 Hamamatsu photomultiplier). The excitation source was a 200 W mercury−xenon lamp (Hamamatsu). The excitation wavelength was set to 280 nm by a grating monochromator (Kratos GM 252, Polytec). No photobleaching was observed under the applied experimental conditions. The emission signal was selected by a 3 mm thick 345 nm cutoff filter (Schott). An instrumental dead time of 1.6 ± 0.2 ms was determined by employing the reaction of *N*-bromosuccinimide and *N*-acetyl-L-tryptophanamide as previously described (*37*). We used Kloehn syringes supplying equal volumes of ca. 50 μL of both solutions for the mixing process. To induce mixing, a pressure of 6 bar was applied. The cell unit was thermostated at 20 ± 0.2 °C. Unless specified differently, all reported concentrations of reactants correspond to those after mixing. Pseudo-first-order conditions were ensured by applying $Zn^{2+}$ concentrations that were at least 10-fold higher than the peptide concentration. In this way, the formation of a 2:1 complex (two peptide ligands per cation) that may occur under conditions where the peptide concentration is much higher than that of metal cation (*38*, *39*) is excluded, and only the formation of a 1:1 complex for both peptides needs to be considered. The range of applied total $Zn(ClO_4)_2$ concentrations was dependent on pH and ranged between 15 μM and 20 mM. At the overlapping pH values of 5.6 and 6.8, the measurements were

carried out in two different buffers to check for potential buffer effects. No inconsistency in the $k_{obs}$ values greater than 10% was observed. For every set of concentrations, typically, four to seven individual time courses were recorded under the same experimental conditions. Because of instrumental dead time limitations, only $k_{obs}$ values up to ~400 $s^{-1}$ were considered.

To perform the kinetic experiments under anaerobic conditions, the stopped-flow apparatus was used in a home-built setup consisting of a glovebox containing an atmosphere of purified nitrogen (quality, 4.6).

*Calculation of the Outer-Sphere Equilibrium Binding Constant.* The equilibrium binding constant of the outer sphere complex, $K_{os}$, can be calculated according to the equation derived in ref *40* for electrostatic point charges in dilute solution (*41*)

$$K_{os} = \frac{4\pi}{3000} r^3 N_A e^{-\Phi/k_B T} \quad (1a)$$

with

$$\Phi = \frac{z_+ z_- q_e^2}{Dr} - \frac{z_+ z_- q_e^2 \kappa}{D(1+\kappa r)}$$

$$\kappa = \sqrt{\frac{8\pi N_A q_e^2}{1000 D k_B T} I}$$

where $\Phi$ is the Debye−Hückel interionic potential energy (in erg), $1/\kappa$ is the Debye length (in centimeters), $r$ is the center−center distance between the reactants (reaction distance) in the outer-sphere complex (in centimeters), $N_A$ is Avogadro's number, $z_+$ and $z_-$ are the formal charges of the cation and ligand, respectively, $q_e$ is the elementary charge (in Fr), $k_B T$ is the Boltzmann energy factor (in erg), and $I$ is the ionic strength (in moles per liter). $D$ is the dielectric constant of the solvent, given by the equation $D = \epsilon/\epsilon_0 = \epsilon_{rel}$, where $\epsilon_0$ is the dielectric constant of vacuum. Because this equation refers to ion-pair formation, a neutral ligand constitutes a separate case, which has also been treated in previous studies (*41*−*43*). Indeed, it is obvious that as the ligand charge approaches zero, the exponential term approaches unity and eq 1a is reduced to

$$K_{os} = \frac{4\pi}{3000} r^3 N_A \quad (1b)$$

as derived independently for a diffusion-controlled reaction under no electrostatic interaction conditions (*43*, *44*).

In this context, we can calculate $K_{os}$ values for a variety of ligand charges. In our study, we chose an $r$ of 0.41 nm given by the sum of 0.074 nm, the ionic radius of $Zn^{2+}$ (*45*), and 0.34 nm, the diameter of a water molecule (*46*), separating cation and ligand in the outer-sphere complex.

*Stopped-Flow Dissociation Experiments*. For an independent determination of the dissociation rate constant $k_{off}$, dilution stopped-flow experiments were carried out at pH ≤6.4 by using the instrumentation described above. The solution of the preformed $Zn^{2+}$−peptide complex in a 1 mL syringe was mixed with buffer solution in a 2.5 mL syringe. The dilution factor under these conditions was 3.5. For a one-step reaction with $Zn^{2+}$ in excess and a 3.5-fold dilution, the observed rate constant $k_{obs}$ is given by (*37*)

$$k_{obs} = k_{on}\frac{[Zn^{2+}]_{Tot}}{3.5} + k_{off} \quad (2)$$

which enables the determination of $k_{off}$ from a single experiment, provided the formation rate constant $k_{on}$ is known from previous association measurements (where $[Zn^{2+}]_{Tot}$ is the total $Zn^{2+}$ concentration).

*Kinetic Data Analysis.* The evaluation of the kinetic data for the determination of apparent rate constants $k_{obs}$ and the amplitudes was carried out by including a dead time correction in the form of a corresponding shift of 1.6 ms in the time axis. All time-resolved kinetic phases (association and dissociation experiments) could be analyzed with a monoexponential function. The resulting value for $k_{obs}$, which represents the reciprocal decay time, is given as the arithmetic mean together with the standard deviation of the corresponding data set. All fitting procedures were carried out with Microcal Origin version 6.1 based on the nonlinear least-squares method applying the Levenberg−Marquardt algorithm.

All equilibrium constants are expressed here as association constants $K$ (reciprocal of dissociation constant $K_{Diss}$). With regard to protonation−deprotonation equilibria, this implies that the value of log $K$ corresponds to that of p$K_{Diss}$.

## RESULTS

### *Ser49(35−50)NCp7*

*Kinetic Analysis at a Single pH Value.* The dynamics of binding of $Zn^{2+}$ to Ser49(35−50)NCp7 (Chart 1) was investigated at pH 6.0, 20 °C, and a constant ionic strength under pseudo-first-order conditions by employing the anaerobic fluorescence stopped-flow technique. A single time-resolvable fluorescence intensity increase was observed upon the rapid mixing of the peptide with $Zn(ClO_4)_2$ solutions of different concentrations. In Figure 1 (inset), the measured time course upon the rapid mixing of 1.5 $\mu$M Ser49(35−50)NCp7 with 0.2 mM $Zn(ClO_4)_2$ in 50 mM MES/NaOH (pH 6.0) at a total ionic strength of 0.15 M (adjusted with $NaClO_4$) is shown as a representative example. The resolved kinetic phase could be fitted with a monoexponential function. The experimentally determined dead time was taken into account for the determination of all $k_{obs}$ values and amplitudes by extrapolating the kinetic phase to the true time zero (see Materials and Methods). No initial fast amplitude change, corresponding to a not time-resolved kinetic phase, was observed. The kinetic experiments carried out at a given pH but at different concentrations of $Zn^{2+}$ provided linear concentration dependences of $k_{obs}$ (Figure 1). The amplitude of the resolved phase under the chosen conditions was essentially independent of $Zn(ClO_4)_2$ concentrations because almost all free peptide was converted to its metal complex. Since protonation−deprotonation reactions of the peptide and its cation complexes in buffered solution are very fast (*47*), we assume that these reactions are more than 1 order of magnitude faster than the stopped-flow mixing time. Therefore, the resolvable process is attributed to binding of $Zn^{2+}$ by the peptide. On the basis of the simplest possible kinetic one-step binding scheme, where all deprotonation reactions

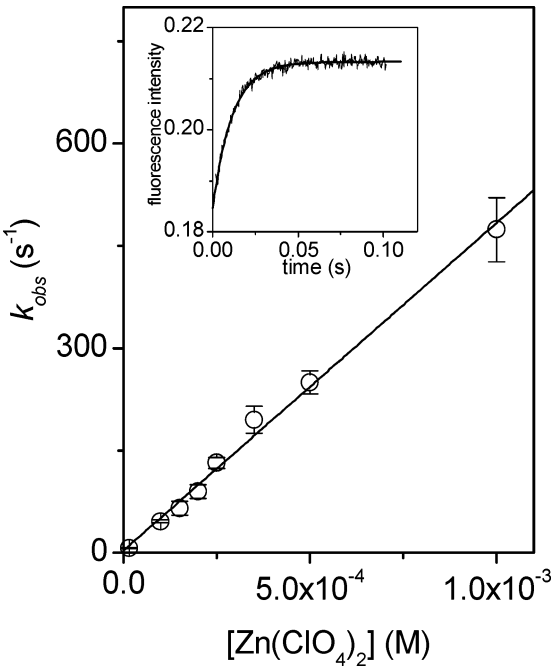


FIGURE 1: Typical example of the kinetics of binding of $Zn^{2+}$ to Ser49(35−50)NCp7 (1.5 $\mu$M) at 20 °C in 50 mM MES/NaOH (pH 6.0) at a total ionic strength of 0.15 M. Dependence of observed rate constant $k_{obs}$ vs total zinc concentration. The solid line is the best fit of the data according to eq 3 for which $k_{on} = (4.9 \pm 0.2) \times 10^5$ $M^{-1}$ $s^{-1}$ and $k_{off} = 3 \pm 1$ $s^{-1}$. The inset shows a representative kinetic experiment of the rapid mixing between 1.5 $\mu$M Ser49(35−50)NCp7 and 0.2 mM $Zn(ClO_4)_2$. The solid line represents the best fit by a monoexponential function with $k_{obs} = 85$ $s^{-1}$. A dead time of 1.6 ms was taken into account (see Materials and Methods). The concentrations refer to conditions after mixing.

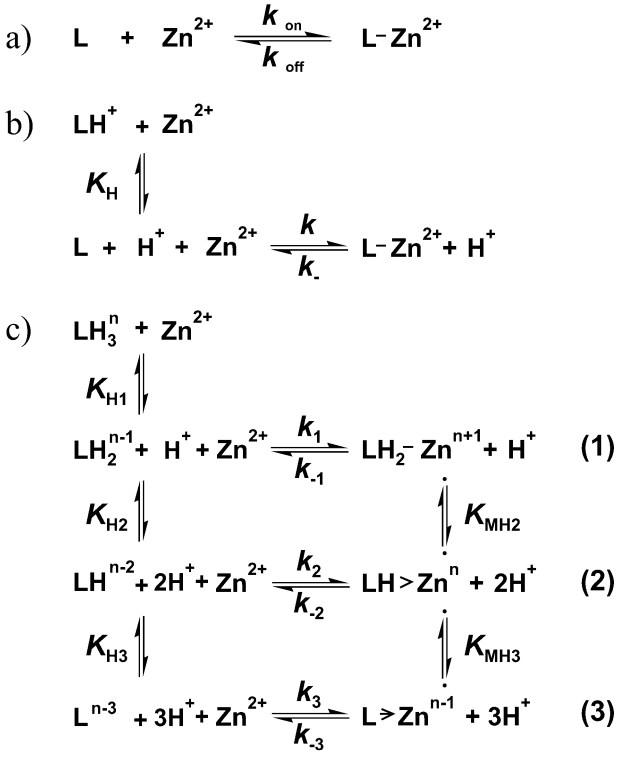


FIGURE 2: Kinetic reaction schemes. (a) Single-step binding reaction scheme where deprotonation reaction steps are omitted. (b) Scheme for a single-step binding reaction, characterized by formation and dissociation rate constants $k$ and $k_-$, respectively, coupled to one preceding deprotonation process, characterized by equilibrium constant $K_H$. (c) General reaction model of binding of $Zn^{2+}$ to Ser49(35−50)NCp7 ($n = 1$) and Ala44(35−50)NCp7 ($n = 0$), where equilibrium constants $K_{Hi}$, expressed as association constants, characterize the deprotonation of the unbound and $K_{MHi}$ those of the zinc-bound ligand; $k_i$ and $k_{-i}$ are the formation and dissociation rate constants, respectively, of the $i$th metal binding step. Binding steps 2 and 3 and in particular both intramolecular coordination steps involve folding elements.

are neglected (Figure 2a), the overall complex formation and dissociation rate constants, $k_{on}$ and $k_{off}$, respectively, can be determined from the linear $Zn(ClO_4)_2$ concentration dependence of $k_{obs}$ under pseudo-first-order conditions

$$k_{obs} = k_{on}[Zn^{2+}] + k_{off} \quad (3)$$

At pH 6.0, we obtained values of $(4.9 \pm 0.2) \times 10^5$ $M^{-1}$ $s^{-1}$ and $3 \pm 1$ $s^{-1}$ for $k_{on}$ and $k_{off}$, respectively (Figure 1). Although the $k_{obs}$ values determined for the highest applied $Zn(ClO_4)_2$ concentrations could have been underestimated because they are close to the reciprocal value of the setup dead time, the deviations from the expected linear concentration dependence according to eq 3 are small. Furthermore, consistency with the simple reaction scheme shown in Figure 2a is confirmed by the fact that the ratio of $k_{on}$ to $k_{off}$, $1.6 \times 10^5$ $M^{-1}$, is close to the overall stability constant of $3.5 \times 10^5$ $M^{-1}$, determined by equilibrium titration (*31*).

*pH Dependence of Kinetic Parameters.* Since deprotonation reactions are assumed to be involved in the $Zn^{2+}$ binding reaction (*29*−*31*), kinetic experiments were carried out between pH 4.7 and 8.5 at 20 °C and at a constant ionic strength. The complex formation rate constant, $k_{on}$, obtained according to eq 3 for different pH values, is plotted versus pH in Figure 3a. The $k_{on}$ values increase with an increase in pH until saturation is reached above pH 8. To describe the observed pH dependency, an expanded kinetic reaction model consisting of a single binding process, coupled to a single preceding deprotonation step as the simplest possibility, is applied first (Figure 2b). An interaction between the fully protonated state $LH^+$ of the coordinating ligand and $Zn^{2+}$ is excluded for electrostatic reasons. This scheme is described by eq 4:

$$k_{on} = \frac{k}{1 + \frac{K_H}{10^{pH}}} \quad (4)$$

A fit of the experimental data given in Figure 3a shows good consistency only at pH ≥6.0 and leads to a value for formation rate constant $k$ of $(5 \pm 2) \times 10^7$ $M^{-1}$ $s^{-1}$ and a value for log $K_H$ of $8.1 \pm 0.2$. This log $K_H$ value suggests a major involvement of the Cys36 residue, which is characterized by a deprotonation constant of 8.0 according to $^1H$ NMR pH titrations of (35−50)NCp7 (*30*).

A better and chemically more realistic description of the experimental results, especially below pH 6.0, can be achieved if two successive deprotonation steps prior to coordination are considered. This partial model is introduced on the basis of the general reaction scheme shown in Figure 2c. It involves ligand states $LH_3^+$, $LH_2$, and $LH^-$ together with two subsequent $Zn^{2+}$ binding steps (steps 1 and 2 in

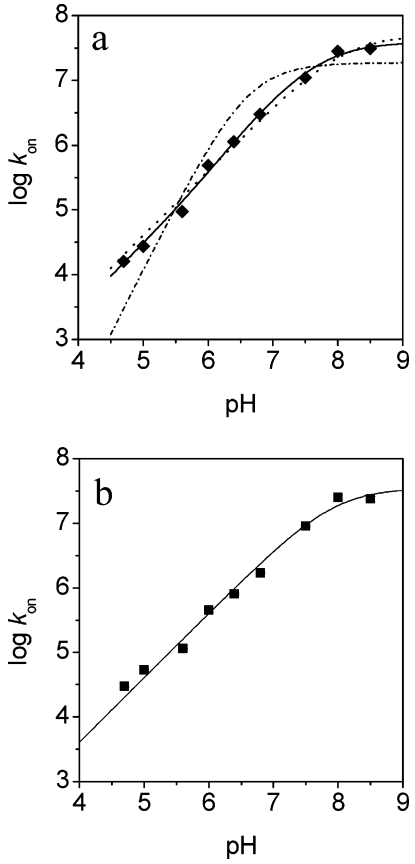


FIGURE 3: pH dependence of the apparent formation rate constant for the $Zn^{2+}$ complex of Ser49(35−50)NCp7 (a) and Ala44(35−50)NCp7 (b). Experiments were performed with a peptide concentration of 1.5 $\mu$M at 20 °C and a total ionic strength of 0.15 M. (a) The dotted line represents the fit to the experimental data using eq 4 which leads to the following: log $K_H = 8.1 \pm 0.2$ and $k = (5 \pm 2) \times 10^7$ $M^{-1}$ $s^{-1}$. The dashed and dotted line represents the fit according to eq 5, with log $K_{H1} = 6.4$ as the fixed parameter and $k_1 = 0$, which leads to log $K_{H2} = 6.8 \pm 0.8$ and $k_2 = (2 \pm 1) \times 10^7$ $M^{-1}$ $s^{-1}$. The solid line corresponds to the fit employing eq 5 with only log $K_{H1}$= 6.4 as the fixed parameter, providing log $K_{H2} = 7.8 \pm 0.1$, $k_1 = (1.0 \pm 0.2) \times 10^6$ $M^{-1}$ $s^{-1}$, and $k_2 = (3.9 \pm 0.8) \times 10^7$ $M^{-1}$ $s^{-1}$. (b) The solid line corresponds to the fit employing eq 5 with log $K_{H1} = 8.0$, log $K_{H2} = 8.8$, and $k_2 = 5.0 \times 10^7$ $M^{-1}$ $s^{-1}$ as fixed parameters, providing $k_1 = (3.6 \pm 0.4) \times 10^7$ $M^{-1}$ $s^{-1}$. Error bars of apparent rate constants below pH 6.2 are of the size of the chosen symbols but smaller above pH 6.2.

Figure 2c). Under these conditions, eq 5 is applied for the fit of the pH dependence of $k_{on}$ (*48*):

$$k_{on} = \frac{k_1 + k_2 \frac{10^{pH}}{K_{H2}}}{1 + \frac{10^{pH}}{K_{H2}} + \frac{K_{H1}}{10^{pH}}} \quad (5)$$

The slope in the low-pH region of the experimental curve in Figure 3a can be adequately described by the additional deprotonation step. However, the available kinetic data below pH 6.5 do not permit a quantitative determination of the corresponding proton dissociation constant $K_{H1}$. On the basis of the results of $^1$H NMR pH titrations of (35−50)NCp7 (*30*), we assign the value of 6.4 to log $K_{H1}$, which mainly accounts for the deprotonation of His44. This value will be applied for all following calculations. Thus, on the basis of eq 5, values of 7.8 ± 0.1 for log $K_{H2}$, $(1.0 \pm 0.2) \times 10^6$ $M^{-1}$ $s^{-1}$ for $k_1$, and $(3.9 \pm 0.8) \times 10^7$ $M^{-1}$ $s^{-1}$ for $k_2$ were obtained. This model does not imply that the His44 side chain must be bound prior to that of Cys36. Under our experimental conditions, it is more likely that bidentate ligand state $LH^-$ binds faster because its rate constant is higher than that of the monodentate state, even if the latter state predominates. Since Cys36 is negatively charged in the bidentate ligand state, it will coordinate before His44 and thus will bind first, representing the corresponding rate-limiting process. Noticeably, an analysis based on a kinetic reaction model consisting of two deprotonation steps of the free ligand, characterized by $K_{H1}$ and $K_{H2}$, but followed only by the single $Zn^{2+}$ binding step 2 is clearly not consistent with the experimental data (dashed and dotted line in Figure 3a). Therefore, this simple model is excluded.

The scheme shown in Figure 2c, comprising all three binding steps, represents the complete reaction scheme expected for a tridentate ligand and is described by the following equation:

$$k_{on} = \frac{k_1 + k_2 \frac{10^{pH}}{K_{H2}} + k_3 \frac{10^{2pH}}{K_{H3}K_{H2}}}{1 + \frac{10^{2pH}}{K_{H3}K_{H2}} + \frac{10^{pH}}{K_{H2}} + \frac{K_{H1}}{10^{pH}}} \quad (6)$$

Unfortunately, the available experimental data do not permit a precise quantitative analysis on the basis of eq 6. Indeed, data points required to accurately determine the $k_3$ value could not be obtained because the binding reaction at pH >8.5 is too fast to be resolved by our setup. To obtain an estimate of $k_3$, simulations were carried out on the basis of eq 6 by setting $k_1$ equal to $1.0 \times 10^6$ $M^{-1}$ $s^{-1}$ and by fixing log $K_{H1}$, log $K_{H2}$, and log $K_{H3}$ to 6.4, 8.0, and 8.9, respectively, as determined by $^1$H NMR pH titrations for (35−50)NCp7. As an upper limit, we found that $k_3$ cannot be larger than $2 \times 10^7$ $M^{-1}$ $s^{-1}$. A similar value for $k_3$ is obtained when log $K_{H2}$ is set to 7.8, which is the value determined by our kinetic analysis (Table 1). This result for $k_3$ contradicts the expectation that for a flexible multidentate ligand, $k_3$ should be significantly larger than $k_2$ as a consequence of the increase in the negative charge of the ligand.

We now consider the reaction paths for $Zn^{2+}$ dissociation. If the overall binding of $Zn^{2+}$ to the model peptide is analyzed as a one-step binding equilibrium under conditions where deprotonation steps are omitted, we can easily calculate the overall dissociation rate constants $k_{off}$ for different pH values, provided the related formation rate and equilibrium binding constants are known. Values calculated in this manner are illustrated in Figure 4a. Experimental $k_{off}$ values, resulting either from the intercept of the $Zn(ClO_4)_2$ concentration dependencies of $k_{obs}$ (provided $k_{off} > 0.1$ $s^{-1}$) or from time-resolved dissociation experiments, are in good agreement with the calculated ones. The linear part of the curve in Figure 4a is characterized by a slope of 2.0 ± 0.2, indicating that at least two acidic groups control the dissociation of $Zn^{2+}$. This conclusion is consistent with the reaction scheme in Figure 2c under the condition that the dissociation process via step 3 is ignored due to an excessively low $k_{-3}$ value, and dissociation occurs mainly via $k_{-1}$. The two dissociation rate constants, $k_{-1}$ and $k_{-2}$, together

Table 1: Kinetic Parameters for the Binding of $Zn^{2+}$ to Ser49(35−50)NCp7 and Ala44(35−50)NCp7, Related to the Extended Reaction Scheme in Figure 2c

| | step (*i*) | log $K_{Hi}$ | log $K_{Mi}$[c] | $k_i$ ($M^{-1}$ $s^{-1}$) | $k_{-i}$ ($s^{-1}$) | log $K_{MHi}$[d] |
|---|---|---|---|---|---|---|
| Ser49(35−50)NCp7 | 1 | −[a] (6.4[b]) | ≤2.3 | $(1.0 \pm 0.2) \times 10^6$ | ≥1000 | − |
| | 2 | $7.8 \pm 0.1$ (8.0[b]) | $7.2 \pm 0.2$ | $(3.9 \pm 0.8) \times 10^7$ | $0.3 \pm 0.2$ | ≤4[b] |
| | 3 | −[a] (8.9[b]) | $12.0 \pm 0.1$ | $\leq 2.0 \times 10^7$ | $\leq 10^{-6}$ | 4.3[b] |
| Ala44(35−50)NCp7 | 1 | $7.9 \pm 0.2$ (8.0[b]) | ≤4.8 | $(3.6 \pm 0.4) \times 10^7$ | $500 \pm 100$ | |
| | 2 | −[a] (8.8[b]) | $9.8 \pm 0.1$ | $\leq 5.0 \times 10^7$ | $(4 \pm 8) \times 10^{-3}$ | ≤4[b] |
| | 3 | −[a] (9.4[b]) | $14.2 \pm 0.1$ | −[a] | $\leq 10^{-6}$ | 5.0[b] |

[a] Not determined. [b] Values derived from equilibrium titrations (*31*). [c] log $K_{Mi}$ values characterize the binding steps as reported in ref *31*. [d] log $K_{MHi}$ values characterize deprotonation and subsequent metal coordination in the final states of the complex.

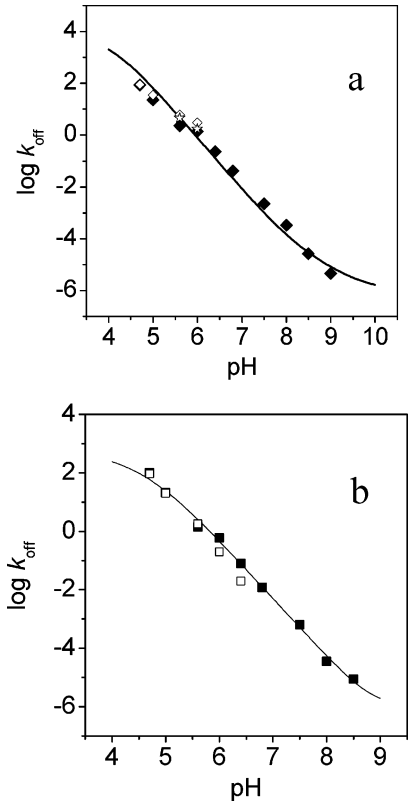


FIGURE 4: pH dependence of the apparent dissociation rate constant of the $Zn^{2+}$ complex with Ser49(35−50)NCp7 (a) and Ala44(35−50)NCp7 (b). Experimental conditions are as described in the legend of Figure 3. Filled symbols (◆ and ■) correspond to $k_{off}$ values calculated from the relation $k_{off} = k_{on}/K$. Empty symbols (◇ and □) or stars (☆) correspond to $k_{off}$ values determined experimentally from the intercepts of the dependence of $k_{on}$ on total zinc concentration or by carrying out dilution jump experiments, respectively. In panel a, the solid line represents the best simulation using eq 8 with $k_{-1} = 8000$ $s^{-1}$ and $k_{-2} = 0.3 \pm 0.2$ $s^{-1}$ together with the fixed parameters $k_{-3} = 10^{-6}$ $s^{-1}$, log $K_{MH2} = 3.7$, and log $K_{MH3} = 4.3 \pm 0.3$. In panel b, the solid line represents the best simulation using eq 8 with $k_{-1} = 500 \pm 100$ $s^{-1}$ and $k_{-2} = (4 \pm 8) \times 10^{-3}$ $s^{-1}$ together with the fixed parameters $k_{-3} = 10^{-6}$ $s^{-1}$, log $K_{MH2} = 4$, and log $K_{MH3} = 5$.

with the two equilibrium constants, $K_{MH2}$ and $K_{MH3}$, can be determined quantitatively according to eq 7:

$$k_{off} = \frac{k_{-1} + k_{-2}\dfrac{10^{pH}}{K_{MH2}}}{1 + \dfrac{10^{pH}}{K_{MH2}} + \dfrac{10^{2pH}}{K_{MH2}K_{MH3}}} \quad (7)$$

A precise determination of all parameters by applying eq 7 is not possible. However, if we fix a value of 4.3 for log $K_{MH3}$ and assume a lower limit of $10^3$ $s^{-1}$ for $k_{-1}$ according to equilibrium titrations (*31*) and simulations, a $k_{-2}$ value of ∼0.3 $s^{-1}$ results. Moreover, we found an upper limit of 4 for log $K_{MH2}$, the most acidic deprotonation step of the $Zn^{2+}$-bound peptide, in good agreement with equilibrium binding data (*31*). The $K_{MHi}$ values, which characterize a deprotonation step coupled to the subsequent coordination process, are several orders of magnitude larger than the related $K_{Hi}$ values (Table 1).

Finally, if the general model (Figure 2c), comprising all three binding steps, is applied for the analysis of the complete dissociation process, eq 8 is used and an upper limit for $k_{-3}$ of $10^{-6}$ $s^{-1}$ can be estimated. The parameters chosen for the fitting curve in Figure 4a (solid line) are given in Table 1.

$$k_{off} = \frac{k_{-1} + k_{-2}\dfrac{10^{pH}}{K_{MH2}} + k_{-3}\dfrac{10^{2pH}}{K_{MH2}K_{MH3}}}{1 + \dfrac{10^{pH}}{K_{MH2}} + \dfrac{10^{2pH}}{K_{MH2}K_{MH3}}} \quad (8)$$

*Ala 44(35−50)NCp7*

*Kinetic Analysis at a Single pH Value*. A stopped-flow study under the conditions described for Ser49(35−50)NCp7 was performed with Ala44(35−50)NCp7. At pH 6.0, $Zn^{2+}$ binding is characterized by a single time-resolved kinetic phase, providing again a linear $Zn^{2+}$ concentration dependence of $k_{obs}$. The analysis according to eq 3, related to the model shown in Figure 2a, leads to $k_{on}$ and $k_{off}$ values of $(4.5 \pm 0.3) \times 10^5$ $M^{-1}$ $s^{-1}$ and $0.4 \pm 0.2$ $s^{-1}$, respectively. Whereas the $k_{on}$ value is close to that obtained for Ser49(35−50)NCp7 at the same pH, that for $k_{off}$ is lower. This finding is considered to be an expression of the higher $Zn^{2+}$ affinity of this mutant, which contains three Cys residues instead of only two for Ser49(35−50)NCp7. The ratio of $k_{on}$ to $k_{off}$ is very close to the value of the overall stability constant at the same pH (*31*), indicating again consistency between kinetic and equilibrium analysis.

*pH Dependence of Kinetic Parameters*. Also the kinetic parameters obtained for Ala44(35−50)NCp7 exhibit a marked pH dependence. In the simplest possible partial model related to Figure 2b, the fit of the experimental data with eq 4 provides a value for $k$ of $(4 \pm 1) \times 10^7$ $M^{-1}$ $s^{-1}$ together with a log $K_H$ value of $7.9 \pm 0.2$, which is again consistent with a major involvement of the Cys36 residue. If we extend the reaction scheme and assume that two deprotonable acidic groups of Ala44(35−50)NCp7 are involved in the binding of $Zn^{2+}$ (cf. Figure 2c where binding steps 1 and 2 are considered), a value for $k_1$ of $(3.6 \pm 0.4) \times 10^7$ $M^{-1}$ $s^{-1}$ and an upper limit for $k_2$ of $5 \times 10^7$ $M^{-1}$ $s^{-1}$ result from the fit

employing eq 5, with log $K_{H1}$ and log $K_{H2}$ set to 8.0 and 8.8, respectively, according to the $^1$H NMR pH titrations (*30*). The fit based on the extended model is not significantly better than the first one but clearly shows that $k_2$ is similar to $k_1$. As the negative charge of the ligand is increased from $LH_2^-$ to $LH^{2-}$, as a consequence of the deprotonation of the second Cys residue, it is surprising that the value of $k_2$ is not significantly larger than that of $k_1$. The third Cys side chain, attributed to Cys49, is probably not markedly involved in the initial formation of the $Zn^{2+}$ complex because of its very high log $K_{H3}$ value of 9.4 (*30*, *31*). Thus, binding step 3 in Figure 2c, related to the fully deprotonated ligand, will not significantly contribute to complex formation. It is much more likely that the coordination of the third Cys residue occurs by deprotonation of intermediate complex LHZn with subsequent coordination.

If the overall binding of $Zn^{2+}$ to Ala44(35−50)NCp7 is analyzed in the form of a one-step equilibrium, we can also calculate the dissociation rate constant $k_{off}$ for each pH value where the equilibrium constant and formation rate constant $k_{on}$ are known from separate determinations (Figure 4b). Also for this peptide, the experimentally determined dissociation rate constants, resulting either from the intercepts of the $Zn(ClO_4)_2$ concentration dependences of $k_{obs}$ (according to eq 3, provided $k_{off} > 0.1$ s$^{-1}$) or from dilution jump experiments, match the calculated ones, validating the model used for the calculation. The data shown in Figure 4b clearly demonstrate that the dissociation of the final $Zn^{2+}$ complex strongly depends on pH. The linear part of the plot in Figure 4b is characterized by a slope of 2.2 ± 0.2, indicating that two acidic groups participate in the dissociation of $Zn^{2+}$ from its complex as with Ser49(35−50)NCp7. All the determined and estimated parameters are given in Table 1. Dissociation rate constants $k_{-2}$ and $k_{-1}$ are considerably lower than the corresponding ones for Ser49(35−50)NCp7. This is attributed to the greater stability of the complex formed with three deprotonated Cys residues in Ala44(35−50)NCp7.

## DISCUSSION

In this paper, the kinetics of binding of $Zn^{2+}$ to two point mutants of the HIV-1 NCp7 distal finger, Ser49(35−50)NCp7 and Ala44(35−50)NCp7, is studied at different pH values in an attempt to understand the dynamic aspects and the mechanism of metal coordination. Our data clearly indicate that both the rates of binding (Figure 3) and dissociation (Figure 4) are pH-dependent for both peptides. This behavior is interpreted on the basis of the reaction model in Figure 2c, where the heavy metal ion can be bound to three different protonation−deprotonation states of the free ligand. According to this model, two limiting cases for the binding mechanism are considered. Cation binding occurs either in a single step solely via the fully deprotonated and negatively charged binding site (step 3 in Figure 2c) or via a multistep process involving three binding paths due to all three deprotonated ligand states (steps 1−3 in Figure 2c).

In general, ligand coordination by a solvated metal ion is assumed to occur via the fast formation of an outer-sphere complex between the still fully solvated cation and the ligand, characterized by the pre-equilibrium constant $K_{os}$ (eq 1 of Materials and Methods). This step is followed by the usually rate-limiting substitution of the first solvate water molecule by the coordinating atom of the ligand, which leads to inner-sphere coordination (Eigen−Wilkins mechanism). The rate constant of this substitution process, $k_{subst}$, is characteristic of a particular metal ion and is around $3 \times 10^7$ s$^{-1}$ for $Zn^{2+}$ (*42*, *49*). Since the intermediate outer-sphere complex is not markedly populated, the formation of a coordination complex is usually detected in the form of a single reaction step, where the overall formation rate constant corresponds to the product $K_{os}k_{subst}$. Differences between ligands, for example, due to different charges, generally lead to different values of $K_{os}$ but not to significantly different $k_{subst}$ values. For a flexible multidentate ligand, it is generally assumed that the coordination of the first ligand atom, in particular, if it is negatively charged, leads to a weakening of the interaction between the metal ion and the remaining coordinated water molecules. Consequently, any subsequent intramolecular coordination of further ligand atoms under these circumstances will be faster. This requires, however, substantial ligand flexibility because the rearrangement of the ligand conformation, necessary to bring the next coordinating atoms into the required position, must be faster than the subsequent substitution of the remaining solvate water molecules. Thus, the final complex is formed by a stepwise substitution process. In the case of nonflexible ligands, the conformational rearrangement itself can act as the rate-limiting reaction step. Because the charge of the zinc binding site of the peptides investigated here depends sensitively on pH, different protonation states of the coordinating groups differ with regard to their charge and will lead to different $K_{os}$ values and thus to different binding rate constants. These rate constants are expected to increase with an increase in the negative charge of the ligand. For the interaction between an uncharged ligand binding site and a divalent metal ion such as $Zn^{2+}$, a $K_{os}$ value of 0.17 M$^{-1}$ is calculated on the basis of eq 1b under the conditions specified in Materials and Methods. According to ref *40*, values of 1.9, 21.5, and 240 M$^{-1}$ are obtained for the binding of $Zn^{2+}$ to sites with the charges of −1, −2, and −3, respectively. The resulting values for the rate constants are $5 \times 10^6$ for the neutral ligand and $6 \times 10^7$, $6 \times 10^8$, and $7 \times 10^9$ M$^{-1}$ s$^{-1}$, respectively, for the three different negative charges of the binding site. Accordingly, these values would be expected for binding rate constants $k_1$ to $k_3$ (cf. Figure 2c). Although the theoretical considerations of Fuoss (*40*) have been developed for reaction partners with point charges, applications to ligands with distributed charges still provide meaningful estimations (*48*).

*Kinetics of Binding of $Zn^{2+}$ to Ser49(35−50)NCp7.* If binding steps 1 and 2 (Figure 2c) are used for the evaluation of the kinetic data of Ser49(35−50)NCp7, the values of $k_1$ and $k_2$ resulting from the fit are nearly identical with those calculated on the basis of the Fuoss model for a ligand with no and a single negative charge, respectively (Table 1). A realistic assignment of the protonation−deprotonation equilibrium coupled to $Zn^{2+}$ binding step 2 can also be achieved since the log $K_{H2}$ value of 7.8, resulting from the kinetic study, can be clearly attributed to the deprotonation of Cys36 on the basis of the experimentally determined ionization constants of (35−50)NCp7 and Ala44(35−50)NCp7 (*30*, *31*). The more acidic deprotonation step associated with log $K_{H1}$ is assigned to His44.

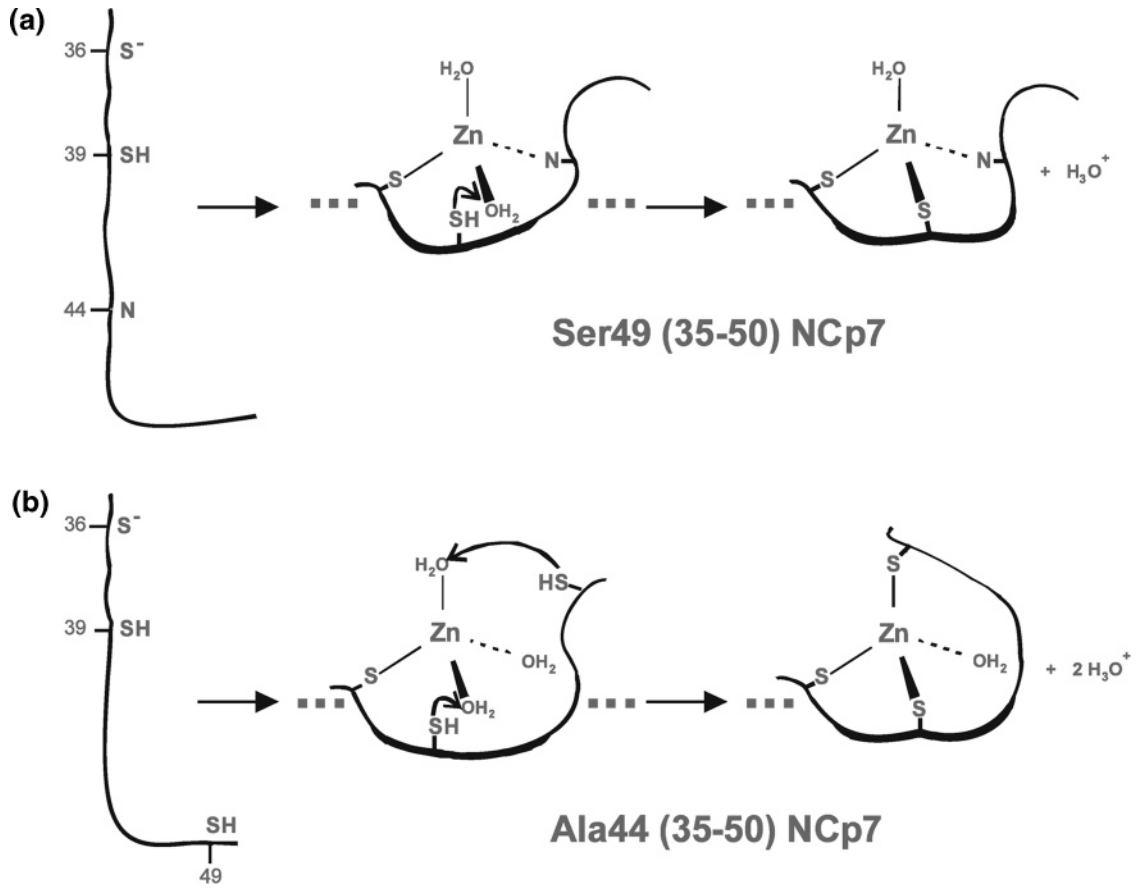


FIGURE 5: Proposed mechanism of $Zn^{2+}$ coordination by Ser49(35−50)NCp7 and Ala44(35−50)NCp7 in the neutral pH range. Only one selected but major intermediate state, relevant for $Zn^{2+}$ binding and dissociation, is shown for each peptide.

Since rate constants $k_1$ and $k_2$ (Table 1) display the expected values according to their charge for a simple, flexible, and multidentate ligand, there is no evidence for a slow conformational ligand rearrangement involved in the corresponding coordination processes. In contrast, the estimated value of $k_3$ (upper limit of $2 \times 10^7$ $M^{-1}$ $s^{-1}$) is even smaller than that of $k_2$, indicating that at pH >8, the expected contribution of a faster complex formation path related to $Zn^{2+}$ binding step 3 in Figure 2c, where both deprotonated Cys residues are involved, is not observed. This suggests that the uncomplexed, fully deprotonated Ser49(35−50)-NCp7 peptide neither exhibits the coordination properties of a very flexible multidentate ligand such as EDTA nor exists in a preorganized conformation similar to that of the peptide in the $Zn^{2+}$ complex of the C-terminal NCp7 finger motif, in line with NMR studies (*3*, *5*, *9*). Both prerequisites would be expected to provide the conditions of a very fast complexation process. Thus, the unexpectedly slow $k_3$ value may be attributed to conformational constraints in the tridentate ligand that do, however, not lead to the population of a stable reaction intermediate. Consequently, the fastest reaction path to reach the final complex LZn of Ser49(35−50)NCp7 in the investigated pH range occurs via intermediate state $LHZn^+$, and not via the intermolecular binding process, $k_3$.

Since the reaction mechanism involved here cannot be attributed to a simple single-step process (step 3 in Figure 2c) or to a complete multistep binding process (steps 1−3), the mechanism is due to a multistep reaction involving $Zn^{2+}$ binding by the monodentate and bidentate ligand states of the free peptide. The substitution of a solvate water molecule is thought to be rate-limiting for the steps characterized by $k_1$ and $k_2$, while the intramolecular transition from $LHZn^+$ to final complex LZn appears to be very fast.

To identify the most efficient and therefore the major binding path for Ser49(35−50)NCp7, we have to consider not only the determined rate constants (Table 1) but also the resulting reaction velocity, which among other parameters, also depends on the concentration and pH-dependent population of the protonation states of the free ligand. Because of unfavorable electrostatics, the binding reaction initiated by the interaction between the positively charged $LH_3^+$ and $Zn^{2+}$ has already been ruled out. Furthermore, below pH 8 a substantial involvement of $L^{2-}$ in the $Zn^{2+}$ association has been neglected, too. Thus, between pH 6 and 8, the reaction will primarily proceed via monodentate and bidentate ligand states $LH_2$ and $LH^-$, respectively (steps 1 and 2 in Figure 2c). If both the Ser49(35−50)NCp7 and $Zn^{2+}$ concentrations are lower than $10^{-4}$ M and the pH is above 6.5, the deprotonated His residue alone cannot markedly coordinate $Zn^{2+}$ and thus does not initiate the coordination process because of its low affinity. Under these conditions, the coordination process will preferentially start via the binding between $Zn^{2+}$ and the $LH^-$ state, which acts as a bidentate ligand (step 2 in Figure 2c and the first binding step in Figure 5a). The final complex is then formed by an intramolecular substitution reaction (second binding step in Figure 5a). However, below pH 6.5, if either the peptide or $Zn^{2+}$ concentration or both concentrations are high ($>10^{-4}$ M) as well as above pH 6.5 under the condition of low $Zn^{2+}$

but with a high peptide concentration, the binding process can be initiated by the coordination of the His44 side chain (step 1 in Figure 2c). The remaining coordination steps can then take place subsequently in a stepwise manner. At very high pH, the coordination of $Zn^{2+}$ is assumed to occur via $L^{2-}$ (step 3 in Figure 2c) and a true one-step binding mechanism will then predominate.

Also, the release of $Zn^{2+}$ from final complex LZn of Ser49(35−50)NCp7 does not occur in a single dissociation step involving $k_{-3}$ (Figure 2c) because its value of $\sim 10^{-6}$ $s^{-1}$ (Table 1) is much too low compared to the rate constants of the multistep dissociation process proceeding via intermediate states $LHZn^{+}$ and $LH_2Zn^{2+}$. The corresponding $Zn^{2+}$ dissociation rate constants $k_{-1}$ and $k_{-2}$ are higher by orders of magnitude (Table 1). Both rate constants represent rate-limiting dissociation steps because the adjustment of equilibria involving protonation and/or deprotonation reactions is assumed to be very fast in buffer solution.

*Kinetics of Binding of $Zn^{2+}$ to Ala44(35−50)NCp7.* The general $Zn^{2+}$ binding mechanism of Ala44(35−50)NCp7 is similar to that of Ser49(35−50)NCp7, except that, according to our kinetic results and in line with the $pK_a$ values of the three Cys residues (*30*, *31*), binding below pH 8.5 is restricted to the intermolecular and thus direct coordination of only two of the three available Cys residues (steps 1 and 2 in Figure 2c). Consequently, the third Cys residue is coordinating by an intramolecular substitution process via intermediate complex LHZn. No direct intermolecular binding between the fully deprotonated site and the heavy metal ion (step 3 in Figure 2c) is observed under our conditions. The value of $3.6 \times 10^7$ $M^{-1}$ $s^{-1}$ for $k_1$ is very close to the theoretical value calculated for the binding between a negatively charged monodentate ligand and $Zn^{2+}$. For the bidentate ligand with two negative charges, a value of $\sim 6 \times 10^8$ $M^{-1}$ $s^{-1}$ is expected, but a value for $k_2$ of only $5 \times 10^7$ $M^{-1}$ $s^{-1}$, close to that of $k_1$, is found experimentally. As for the interpretation of the $k_3$ value in the case of Ser49(35−50)NCp7, we postulate that the relatively slow $Zn^{2+}$ coordination by the bidentate state of Ala44(35−50)NCp7 is due to a rate-limiting conformational ligand rearrangement such as folding, occurring after the coordination of the first Cys residue. Again, no additional, stable intermediate state has been observed for this peptide. Consequently, the binding mechanism of Ala44(35−50)NCp7 is attributed to a multistep reaction involving one major $Zn^{2+}$ binding path due to the monodentate ligand state of the peptide.

At neutral pH, the binding reaction proceeds via the $LH_2Zn^{+}$ state (Figure 2c), which corresponds to the schematic structure of the intermediate shown in Figure 5b. The final, tetrahedral complex (Figure 5b) is then formed upon two fast subsequent deprotonation and intramolecular substitution processes. In a recent molecular simulation study, water molecules were shown to remain in the first solvation sphere of $Zn^{2+}$ and further stabilize the complex with Ala44(35−50)NCp7 by forming H-bonds to the polypeptide chain (*50*). This water−peptide interaction may play a role in folding by reducing the mobility and allowing the local rearrangement that is necessary for formation of the native structure.

Finally, as for Ser49(35−50)NCp7, the value of $k_{-3}$ is again much lower than those of $k_{-2}$ and $k_{-1}$ (Table 1). Therefore, a multistep dissociation of the heavy metal ion via intermediate complexes LHZn and $LH_2Zn^{+}$ (Figure 2c) is also the most likely dissociation pathway for Ala44(35−50)NCp7. All determined dissociation rate constants are lower than the corresponding ones for Ser49(35−50)NCp7, in line with the stronger affinity of Ala44(35−50)NCp7 for $Zn^{2+}$ because of its three Cys residues. It follows that the $Zn^{2+}$ complex of Ala44(35−50)NCp7 has a longer lifetime and consequently a slower decay than that of Ser49(35−50)NCp7.

## CONCLUSION

In a less detailed kinetic study, the interaction between a tetradentate CCHH motif peptide and mainly $Co^{2+}$ has been studied at a single pH of 7.0. The results have been interpreted on the basis of a single binding equilibrium (*28*). The formation rate constant $k_{on}$ for $Zn^{2+}$ binding, obtained from a kinetic competition study, is considerably higher than what we found for our two (35−50)NCp7 mutants at the same pH (Figure 3). This result is surprising because one would expect larger conformational constraints for coordination for the tetradentate than for the tridentate ligand investigated here. However, it is difficult to draw final mechanistic conclusions from this difference on the basis of the available data and without knowing the equilibrium constants for the deprotonation of the CCHH motif.

Our kinetic results clearly show that heavy metal ion binding to zinc finger motifs can be treated as one-step binding reaction only under very special, nonphysiological conditions. Whether binding is initiated by the peptide in the form of a monodentate or bidentate ligand state depends on the ionization constants of the involved coordinating groups and thus on pH, but also on the stability constant of intermediate complex $LH_2Zn^{n+1}$ (Figure 2c) as well as on the chosen concentrations. Dissociation of $Zn^{2+}$ occurs as a multistep process via the intermediate complexes ($LH_2Zn^{n+1}$ and $LHZn^{n}$ in Figure 2c) and not by a direct dissociation of the heavy metal ion from fully deprotonated, tridentate ligand state $LZn^{n-1}$. This result may be of physiological interest because the dissociation mechanism reported here enables a relatively fast decay of the $Zn^{2+}$−peptide complexes with a half-life time of up to minutes, whereas it would be longer than 200 h if $k_{-3}$ were limiting for the rate of $Zn^{2+}$ dissociation. This dynamic aspect, which is linked to the sequence of the apopeptide, could be even more pronounced for native zinc finger systems and may be of regulatory importance, acting as an evolutionary advantage.

With the increasing degree of deprotonation of the uncomplexed ligand, the binding rate constants do not systematically increase as expected from simple electrostatic considerations. This finding is attributed to conformational constraints. Thus, depending on the chosen peptide, the substitution of a coordinated water molecule appears to be truly rate-limiting only for the initial binding paths (step 1 and/or step 2 in Figure 2c). It would be of fundamental interest to know whether the dynamic and mechanistic properties will change if the complete CCHC motif of the intact (35−50)NCp7 peptide could be investigated in a corresponding manner.

## ACKNOWLEDGMENT

We thank P. Buet and E. Lewitzki for support and helpful discussions and P. Petitjean for peptide systhesis.

## REFERENCES


1. Vallee, B. L., and Auld, D. S. (1990) Zinc coordination, function, and structure of zinc enzymes and other proteins, *Biochemistry 29*, 5647−5659.
2. Parraga, G., Horvath, S. J., Eisen, A., Taylor, W. E., Hood, L., Young, E. T., and Klevit, R. E. (1988) Zinc-dependent structure of a single-finger domain of yeast ADR1, *Science 241*, 1489−1492.
3. Summers, M. F., Henderson, L. E., Chance, M. R., Bess, J. W., Jr., South, T. L., Blake, P. R., Sagi, I., Perez-Alvarado, G., Sowder, R. C. d., Hare, D. R., et al. (1992) Nucleocapsid zinc fingers detected in retroviruses: EXAFS studies of intact viruses and the solution-state structure of the nucleocapsid protein from HIV-1, *Protein Sci. 1*, 563−574.
4. Morellet, N., Jullian, N., De Rocquigny, H., Maigret, B., Darlix, J. L., and Roques, B. P. (1992) Determination of the structure of the nucleocapsid protein NCp7 from the human immunodeficiency virus type 1 by $^1$H NMR, *EMBO J. 11*, 3059−3065.
5. Morellet, N., de Rocquigny, H., Mely, Y., Jullian, N., Demene, H., Ottmann, M., Gerard, D., Darlix, J. L., Fournie-Zaluski, M. C., and Roques, B. P. (1994) Conformational behaviour of the active and inactive forms of the nucleocapsid NCp7 of HIV-1 studied by $^1$H NMR, *J. Mol. Biol. 235*, 287−301.
6. Berg, J. M., and Godwin, H. A. (1997) Lessons from zinc-binding peptides, *Annu. Rev. Biophys. Biomol. Struct. 26*, 357−371.
7. Berg, J. M. (1986) Potential metal-binding domains in nucleic acid binding proteins, *Science 232*, 485−487.
8. Berg, J. M., and Shi, Y. (1996) The galvanization of biology: A growing appreciation for the roles of zinc, *Science 271*, 1081−1085.
9. South, T. L., Blake, P. R., Hare, D. R., and Summers, M. F. (1991) C-Terminal retroviral-type zinc finger domain from the HIV-1 nucleocapsid protein is structurally similar to the N-terminal zinc finger domain, *Biochemistry 30*, 6342−6349.
10. Green, L. M., and Berg, J. M. (1989) A retroviral Cys-Xaa$_2$-Cys-Xaa$_4$-His-Xaa$_4$-Cys peptide binds metal ions: Spectroscopic studies and a proposed three-dimensional structure, *Proc. Natl. Acad. Sci. U.S.A. 86*, 4047−4051.
11. Darlix, J. L., Lapadat-Tapolsky, M., de Rocquigny, H., and Roques, B. P. (1995) First glimpses at structure−function relationships of the nucleocapsid protein of retroviruses, *J. Mol. Biol. 254*, 523−537.
12. Roques, B. P., Morellet, N., de Rocquigny, H., Demene, H., Schueler, W., and Jullian, N. (1997) Structure, biological functions and inhibition of the HIV-1 proteins Vpr and NCp7, *Biochimie 79*, 673−680.
13. de Rocquigny, H., Petitjean, P., Tanchou, V., Decimo, D., Drouot, L., Delaunay, T., Darlix, J. L., and Roques, B. P. (1997) The zinc fingers of HIV nucleocapsid protein NCp7 direct interactions with the viral regulatory protein Vpr, *J. Biol. Chem. 272*, 30753−30759.
14. Druillennec, S., Caneparo, A., de Rocquigny, H., and Roques, B. P. (1999) Evidence of interactions between the nucleocapsid protein NCp7 and the reverse transcriptase of HIV-1, *J. Biol. Chem. 274*, 11283−11288.
15. Cimarelli, A., and Darlix, J. L. (2002) Assembling the human immunodeficiency virus type 1, *Cell. Mol. Life Sci. 59*, 1166−1184.
16. Bernacchi, S., Stoylov, S., Piemont, E., Ficheux, D., Roques, B. P., Darlix, J. L., and Mely, Y. (2002) HIV-1 nucleocapsid protein activates transient melting of least stable parts of the secondary structure of TAR and its complementary sequence, *J. Mol. Biol. 317*, 385−399.
17. Aldovini, A., and Young, R. A. (1990) Mutations of RNA and protein sequences involved in human immunodeficiency virus type 1 packaging result in production of noninfectious virus, *J. Virol. 64*, 1920−1926.
18. Dorfman, T., Luban, J., Goff, S. P., Haseltine, W. A., and Gottlinger, H. G. (1993) Mapping of functionally important residues of a cysteine-histidine box in the human immunodeficiency virus type 1 nucleocapsid protein, *J. Virol. 67*, 6159−6169.
19. Déméné, H., Dong, C. Z., Ottmann, M., Rouyez, M. C., Jullian, N., Morellet, N., Mély, Y., Darlix, J. L., Fournié-Zaluski, M. C., Saragosti, S., and Roques, B. P. (1994) $^1$H NMR structure and biological studies of the His23 → Cys mutant nucleocapsid protein of HIV-1 indicate that the conformation of the first zinc finger is critical for virus infectivity, *Biochemistry 33*, 11707−11716.
20. Gorelick, R. J., Nigida, S. M., Jr., Bess, J. W., Jr., Arthur, L. O., Henderson, L. E., and Rein, A. (1990) Noninfectious human immunodeficiency virus type 1 mutants deficient in genomic RNA, *J. Virol. 64*, 3207−3211.
21. Gorelick, R. J., Gagliardi, T. D., Bosche, W. J., Wiltrout, T. A., Coren, L. V., Chabot, D. J., Lifson, J. D., Henderson, L. E., and Arthur, L. O. (1999) Strict conservation of the retroviral nucleocapsid protein zinc finger is strongly influenced by its role in viral infection processes: Characterization of HIV-1 particles containing mutant nucleocapsid zinc-coordinating sequences, *Virology 256*, 92−104.
22. Guo, J., Wu, T., Anderson, J., Kane, B. F., Johnson, D. G., Gorelick, R. J., Henderson, L. E., and Levin, J. G. (2000) Zinc finger structures in the human immunodeficiency virus type 1 nucleocapsid protein facilitate efficient minus- and plus-strand transfer, *J. Virol. 74*, 8980−8988.
23. Rice, W. G., Turpin, J. A., Schaeffer, C. A., Graham, L., Clanton, D., Buckheit, R. W., Jr., Zaharevitz, D., Summers, M. F., Wallqvist, A., and Covell, D. G. (1996) Evaluation of selected chemiotypes in coupled cellular and molecular target-based screens identifies novel HIV-1 finger inhibitors, *J. Med. Chem. 39*, 3606−3616.
24. Tummino, P. J., Scholten, J. D., Harvey, P. J., Holler, T. P., Maloney, L., Gogliotti, R., Domagala, J., and Hupe, D. (1996) The in vitro ejection of zinc from human immunodeficiency virus (HIV) type 1 nucleocapsid protein by disulfide benzamides with cellular anti- HIV activity, *Proc. Natl. Acad. Sci. U.S.A. 93*, 969−973.
25. Yu, X., Hathout, Y., Fenselau, C., Sowder, R. C., II, Henderson, L. E., Rice, W. G., Mendeleyev, J., and Kun, E. (1995) Specific disulfide formation in the oxidation of HIV-1 zinc finger protein nucleocapsid p7, *Chem. Res. Toxicol. 8*, 586−590.
26. Huang, M., Maynard, A., Turpin, J. A., Graham, L., Janini, G. M., Covell, D. G., and Rice, W. G. (1998) Anti-HIV agents that selectively target retroviral nucleocapsid protein zinc fingers without affecting cellular zinc finger proteins, *J. Med. Chem. 41*, 1371−1381.
27. Frankel, A. D., Berg, J. M., and Pabo, C. O. (1987) Metal-dependent folding of a single zinc finger from transcription factor IIIA, *Proc. Natl. Acad. Sci. U.S.A. 84*, 4841−4845.
28. Buchsbaum, J. C., and Berg, J. M. (2000) Kinetics of metal binding by a zinc finger peptide, *Inorg. Chim. Acta 297*, 217−219.
29. Mély, Y., De Rocquigny, H., Morellet, N., Roques, B. P., and Gérard, D. (1996) Zinc binding to the HIV-1 nucleocapsid protein: A thermodynamic investigation by fluorescence spectroscopy, *Biochemistry 35*, 5175−5182.
30. Bombarda, E., Morellet, N., Cherradi, H., Spiess, B., Bouaziz, S., Grell, E., Roques, B. P., and Mely, Y. (2001) Determination of the p$K_a$ of the four $Zn^{2+}$-coordinating residues of the distal finger motif of the HIV-1 nucleocapsid protein: Consequences on the binding of $Zn^{2+}$, *J. Mol. Biol. 310*, 659.
31. Bombarda, E., Cherradi, H., Morellet, N., Roques, B. P., and Mely, Y. (2002) $Zn^{2+}$ binding properties of single-point mutants of the C-terminal zinc finger of the HIV-1 nucleocapsid protein: Evidence of a critical role of cysteine 49 in $Zn^{2+}$ dissociation, *Biochemistry 41*, 4312−4320.
32. Segawa, S., and Sugihara, M. (1984) Characterization of the transition state of lysozyme unfolding. II. Effects of the intrachain crosslinking and the inhibitor binding on the transition state, *Biopolymers 23*, 2489−2498.
33. Segawa, S., and Sugihara, M. (1984) Characterization of the transition state of lysozyme unfolding. I. Effect of protein−solvent interactions on the transition state, *Biopolymers 23*, 2473−2488.
34. de Rocquigny, H., Ficheux, D., Gabus, C., Fournie-Zaluski, M. C., Darlix, J. L., and Roques, B. P. (1991) First large scale chemical synthesis of the 72 amino acid HIV-1 nucleocapsid protein NCp7 in an active form, *Biochem. Biophys. Res. Commun. 180*, 1010−1018.
35. Ellman, G. L. (1959) Tissue sulfhydryl group, *Arch. Biochem. Biophys. 82*, 70−77.
36. Riddles, P. W., Blakeley, R. L., and Zerner, B. (1983) Reassessment of Ellman's reagent, *Methods Enzymol. 91*, 49−60.
37. Buet, P., Lewitzki, E., Grell, E., Albrecht-Gary, A. M., Wannowius, K. J., Mass, F., Elias, H., Mundt, A. A., and Dupont, Y. (2001) Concentration jump experiments for the precise determination of rate constants of reverse reactions in the millisecond time range, *Anal. Chem. 73*, 857−863.
38. Shi, Y., Beger, R. D., and Berg, J. M. (1993) Metal binding properties of single amino acid deletion mutants of zinc finger peptides: Studies using cobalt(II) as a spectroscopic probe, *Biophys. J. 64*, 749−753.

39. Michael, S. F., Kilfoil, V. J., Schmidt, M. H., Amann, B. T., and Berg, J. M. (1992) Metal binding and folding properties of a minimalist $Cys_2His_2$ zinc finger peptide, *Proc. Natl. Acad. Sci. U.S.A. 89*, 4796−4800.
40. Fuoss, R. M. (1958) Ionic association. III. The equilibrium between ion pairs and free ions, *J. Am. Chem. Soc. 80*, 5059−5061.
41. Hammes, G. G., and Steinfeld, J. I. (1962) Relaxation spectra of some nickel(II) and cobalt(II) complexes, *J. Am. Chem. Soc. 84*, 4639−4643.
42. Rorabacher, D. B. (1966) The kinetics of formation and dissociation of the monoamine complexes of the divalent, first-row, transition metal ions, *Inorg. Chem. 5*, 1891−1899.
43. Prue, J. E. (1965) Association Constants from Contact Charge-transfer Spectra, *J. Chem. Soc.*, 7534−7535.
44. Benson, S. W. (1960) *The foundations of chemical kinetics*, McGraw-Hill, New York.
45. *Handbook of Chemistry and Physics*, 56th ed., CRC Press, Cleveland, OH.
46. Freier, R. K. (1978) *Aqueous solution*, Vol. 2, Gruyter, Berlin.
47. Eigen, M. (1964) Proton transfer, acid−base catalysis, and enzymatic hydrolysis, *Angew. Chem., Int. Ed. Engl. 3*, 1−19.
48. Bremer, C., Ruf, H., and Grell, E. (1998) Kinetics and mechanism of complex formation between $Mg^{2+}$ and methylthymol blue, *J. Phys. Chem. A 102*, 146−152.
49. Eigen, M., and Tamm, K. (1962) Schallabsorption in Elektrolytlösungen als Folge chemischer Relaxation. 2. Messergebnisse und Relaxationsmechanismen für 2-2-wertige Elektrolyte, *Z. Elektrochem. 66*, 107−121.
50. Stote, R. H., Kellenberger, E., Muller, H., Bombarda, E., Roques, B. P., Kieffer, B., and Mely, Y. (2004) Structure of the His44 → Ala Single Point Mutant of the Distal Finger Motif of HIV-1 Nucleocapsid Protein: A Combined NMR, Molecular Dynamics Simulation, and Fluorescence Study, *Biochemistry 43*, 7687−7697.

BI047349+